

# ON THE MASS FORMULA AND WIGNER AND CURVATURE ENERGY TERMS

G. ROYER

*Laboratoire Subatech, UMR : IN2P3/CNRS-Université-Ecole des Mines,  
4 rue A. Kastler, BP 20722, 44307 Nantes Cedex 03, France,  
E-mail: royer@subatech.in2p3.fr*

(Received September 2, 2021)

*Abstract.* The efficiency of different mass formulas derived from the liquid drop model including or not the curvature energy, the Wigner term and different powers of the relative neutron excess  $I$  has been determined by a least square fitting procedure to the experimental atomic masses assuming a constant  $R_{0,charge}/A^{1/3}$  ratio. The Wigner term and the curvature energy can be used independently to improve the accuracy of the mass formula. The different fits lead to a surface energy coefficient of around 17-18 MeV, a relative sharp charge radius  $r_0$  of 1.22-1.23 fm and a proton form-factor correction to the Coulomb energy of around 0.9 MeV.

*Key words:* Nuclear masses, liquid drop model, Wigner term, curvature energy, charge radius.

## 1 INTRODUCTION

The binding energies of exotic nuclei close to the proton and neutron drip lines or in the superheavy element region are still poorly known and the different predictions do not agree completely. Therefore continuous efforts are still needed to determine the nuclear masses. Within a charged liquid drop approach, semi-macroscopic models including a pairing energy have been firstly advanced to reproduce the experimental nuclear masses [1, 2]. The coefficients of the Bethe-Weizsäcker mass formula have been determined once again recently [3]. To reproduce the irregularity of the masses as functions of  $A$  and  $Z$  partly due to shell closings and proton and neutron number parity, macroscopic-microscopic approaches have been elaborated, mainly the finite-range liquid drop model and the finite-range droplet model [4]. The Thomas-Fermi statistical model with a well-chosen effective interaction [5, 6] has also allowed to reproduced accurately the nuclear masses. Microscopic Hartree-Fock self-consistent theories using mean-fields and Skyrme or Gogny forces and pairing correlations [7, 8] as well as relativistic mean field calculations [9] have also been developed to describe these nuclear masses. Finally, nuclear mass systematics using neural networks have been undertaken recently [10].

The evolution of the nuclear binding energy with deformation and rotation governs the fission, fusion, cluster and  $\alpha$  decay potential barriers and the

characteristics of the large deformed rotating states. One or two-body shape sequences have to be selected to simulate the exit or entrance channels [11] in the macroscopic-microscopic models. Within a generalized liquid drop model and a quasi-molecular shape sequence the main features of these barriers have been reproduced using, firstly, four basic macroscopic terms : the volume, surface, Coulomb and nuclear proximity energy contributions and, secondly, shell and pairing energy terms to explain structure effects and improve quantitatively the results [12, 13, 14, 15, 16, 17].

The purpose of the present work is to determine the efficiency of different combinations of terms of the liquid drop model by a least square fitting procedure to the experimentally available atomic masses [18] and to study, particularly, the separated influence of the Wigner term, the curvature energy and different powers of the relative neutron excess  $I$  to improve the GLDM.

## 2 NUCLEAR BINDING ENERGY

The nuclear binding energy  $B_{nucl}(A,Z)$  which is the energy needed to separate all the nucleons forming a nucleus is linked to the nuclear mass  $M_{n.m}$  by

$$B_{nucl}(A, Z) = Zm_P + Nm_N - M_{n.m}(A, Z). \quad (1)$$

This quantity may be connected to the experimental atomic masses given in [18] since :

$$M_{n.m}(A, Z) = M_{a.m}(A, Z) - Zm_e + B_e(Z). \quad (2)$$

The binding energy  $B_e(Z)$  of all removed electrons is determined by [19]

$$B_e(Z) = a_{el}Z^{2.39} + b_{el}Z^{5.35}, \quad (3)$$

with  $a_{el} = 1.44381 \times 10^{-5}$  MeV and  $b_{el} = 1.55468 \times 10^{-12}$  MeV.

The following expansion of the nuclear binding energy in powers of  $A^{-1/3}$  and  $I = (N - Z)/A$  has been considered :

$$\begin{aligned} B = & a_v \left(1 - k_{v_1}|I| - k_{v_2}I^2 - k_{v_3}I^4\right) A - a_s \left(1 - k_{s_1}|I| - k_{s_2}I^2 - k_{s_3}I^4\right) A^{\frac{2}{3}} \\ & - a_k \left(1 - k_{k_1}|I| - k_{k_2}I^2 - k_{k_3}I^4\right) A^{\frac{1}{3}} - a_0A^0 - \frac{3}{5} \frac{e^2 Z^2}{r_0 A^{\frac{1}{3}}} + f_p \frac{Z^2}{A} \\ & - W|I| + E_{pair} - E_{shell} - E_{cong}. \end{aligned} \quad (4)$$

The first term is the volume energy and corresponds to the saturated exchange force and infinite nuclear matter. It includes the asymmetry energy term of the Bethe-Weizsäcker mass formula via the  $I^2A$  term. The second term is the surface energy term. It takes into account the deficit of binding energy of the nucleons at the nuclear surface and corresponds to semi-infinite

nuclear matter. In the Bethe-Weizsäcker mass formula the dependence of the surface energy on  $I$  is not considered. The third term, the curvature energy, is a correction to the surface energy appearing when the surface energy is viewed as a result of local properties of the surface and consequently depends on the mean local curvature. This term is taken into account in the Lublin-Strasbourg drop (LSD) model [20], the TF model [6] but not in the FRLDM [4]. The  $A^0$  term appears when the surface term of the liquid drop model is extended to include higher order terms in  $A^{-1/3}$  and  $I$ . The fifth term is the Coulomb energy. It gives the decrease of binding energy due to the repulsion between the protons. In the Bethe-Weizsäcker mass formula the proportionality to  $Z(Z-1)$  is preferred. For the charge radius the formula  $R_{0,charge} = r_0 A^{1/3}$  is assumed, a more sophisticated expression has been studied in ref. [21]. The  $Z^2/A$  term is a proton form-factor correction to the Coulomb energy which takes into account the finite size of the protons. The term proportional to  $I$  is the Wigner energy [4, 23] which appears in the counting of identical pairs in a nucleus.

The pairing energy has been determined using

$$\begin{aligned} E_{pair} &= -a_p/A^{1/2} \text{ for odd } Z, \text{ odd } N \text{ nuclei,} \\ E_{pair} &= 0 \text{ for odd } A, \\ E_{pair} &= a_p/A^{1/2} \text{ for even } Z, \text{ even } N \text{ nuclei.} \end{aligned} \quad (5)$$

The  $a_p = 11$  value has been adopted following different fits. More sophisticated expressions exist for this pairing energy [4, 6]. The theoretical shell effects given by the Thomas-Fermi model (7<sup>th</sup> column of the table in [5] and [6]) have been retained since they reproduce correctly the mass decrements from fermium to  $Z = 112$  [22]. They are calculated from the Strutinsky shell-correction method and given for the most stable nuclei in the appendix. The sign for the shell energy term comes from the adopted definition in [5]. It gives a contribution of 12.84 MeV to the binding energy for  $^{208}\text{Pb}$  for example. The congruence energy term is given by :

$$E_{cong} = -10 \text{ MeV } \exp(-4.2|I|). \quad (6)$$

It represents an extra binding energy associated with the presence of congruent pairs in contrast to the pure Wigner expression simply proportional to  $I$  [6].

The masses of the 2027 nuclei verifying the two following conditions have been used to obtain the coefficients of the different expansions by a least square fitting procedure :  $N$  and  $Z$  higher than 7 and the one standard deviation uncertainty on the mass lower than 150 keV [18]. The root-mean-square deviation has been calculated using :

$$\sigma^2 = \frac{\sum [M_{Th} - M_{Exp}]^2}{n}. \quad (7)$$

In Table 1, the improvement of the experimental mass reproduction when additional contributions are added to the basic  $A$ ,  $AI^2$ ,  $A^{2/3}$ ,  $A^{2/3}I^2$ ,  $Z^2/A^{1/3}$  terms is clearly shown (each calculation corresponds to one numbered line). The curvature energy is not taken into account. The introduction of the pairing term and of the proton form factor is obviously needful. In contrast, the congruence energy term does not allow to lower  $\sigma$  at least with the fixed coefficients adopted here (as in the LSD and TF models). When the coefficients before the exponential and the exponent are free the congruence energy tends to the Wigner term since the coefficient before the exponential diminishes while the exponent increases. The constant term seems unnecessary. The  $A^{2/3}|I|$  term is useful to improve the accuracy of the expansion and is more efficient than the  $A^{2/3}I^4$  term. The Wigner term plays the major role to decrease  $\sigma$ . When the Wigner term is taken into account the introduction of the  $A^{2/3}|I|$ ,  $A^{2/3}I^4$  and  $A^0$  terms are ineffective. Thus, the very satisfactory value of  $\sigma = 0.60$  MeV can be reached [4, 8, 20]. The introduction of the Wigner term in a liquid drop model has the main drawback that it leads to an important discontinuity at the transition between one and two-body shapes as in fission or fusion. Indeed, when a single system divides into two parts the Wigner term must be evaluated separately for the two fragments and the results added. Thus for the same value of  $|I|$  (symmetric fission or fusion) the Wigner term will jump at scission to 2 times its original value. The same problem exists for the Congruence energy term.

In Table 2, the efficiency of the curvature energy term with different  $I$  dependences is examined, disregarding the Wigner contribution. The introduction of only one term in  $A^{1/3}$  is ineffective while the addition of  $A^{1/3}I^2$  improves slightly the results. Supplementary terms in  $|I|$  to determine the volume, surface and curvature energies allow to reach  $\sigma=0.59$  MeV. They are still more efficient than  $I^4$  terms. The curvature energy term has the advantage that it is continuous at the scission point at least in symmetric fission. It has the disadvantage that its value (and the sign) lacks of stability.

A good convergency of the volume  $a_v$  and asymmetry volume  $k_v$  constants is observed respectively towards around 15.5 MeV and 1.8 – 1.9 . The variation of the surface coefficient is larger but  $a_s$  evolves around 17-18 MeV. Small values of the surface coefficient favors quasi-molecular or two-body shapes at the saddle-point of the potential barriers while large values of  $a_s$  promote one-body elongated shapes. The value of the proton form factor correction tends to 0.92 MeV (this value has been retained also in the LSD model).

The reduced charge radius  $r_{0,charge}$  converges to 1.22-1.23 fm. This is in full agreement with the set of 799 ground state nuclear charge radii presented in ref. [24]. In this compilation a value of  $0.9542A^{1/3}$  for the rms charge radius is obtained, which leads to  $1.23A^{1/3}$  for the effective sharp charge radius. In

Table 1: Coefficient values (in MeV or fm) as functions of the selected term sets including or not the congruence and pairing energies and corresponding root mean square deviation. The shell energy is taken into account.

$n$	$a_v$	$k_{v_1}$	$k_{v_2}$	$k_{v_3}$	$a_s$
1	14.8504	-	1.55448	-	16.1059
2	15.7826	-	1.6165	-	21.017
3	15.5959	-	1.70507	-	17.1723
4	15.6184	-	1.70459	-	17.242
5	15.5233	-	1.71612	-	18.071
6	15.4285	-	1.71066	-	17.5713
7	15.5718	-	1.60965	1.96584	18.0047
8	15.5919	-0.04582	1.90751	-	17.8069
9	15.447	-	1.84011	-	17.3581
10	15.4647	-0.0049	1.8509	-	17.3894
11	15.5147	-	1.85055	-	17.6976
12	15.4607	-	1.83014	0.14095	17.3706
$n$	$k_{s_1}$	$k_{s_2}$	$k_{s_3}$	$a_0$	$W$
1	-	0.93696	-	-	-
2	-	1.13845	-	-18.253	-
3	-	0.98894	-	-	-
4	-	0.98033	-	-	-
5	-	1.40391	-	-	-
6	-	1.39267	-	1.8569	-
7	-	0.75244	10.56741	-	-
8	-0.283	2.39131	-	-	-
9	-	2.11347	-	-	27.5488
10	-0.03409	2.16959	-	-	25.1137
11	-	2.14699	-	-1.409	29.0793
12	-	2.01948	1.10833	-	26.6425
$n$	<i>Cong</i>	<i>Pairing</i>	$r_0$	$f_p$	$\sigma$
1	y	y	1.2434	2.52888	1.156
2	y	y	1.1595	3.34645	0.936
3	n	n	1.2272	-	1.322
4	n	y	1.2244	-	1.032
5	n	y	1.2066	1.47705	0.687
6	n	y	1.2153	1.39388	0.684
7	n	y	1.2042	1.24476	0.665
8	n	y	1.2049	1.0255	0.628
9	n	y	1.2252	0.95419	0.603
10	n	y	1.2234	0.93536	0.603
11	n	y	1.2195	0.98825	0.601
12	n	y	1.2244	0.91559	0.602

Table 2: Coefficient values (in MeV or fm) as functions of the selected term sets and corresponding root mean square deviation. The shell and pairing energies are taken into account but not the congruence energy and the Wigner term.

$n$	$a_v$	$k_{v_1}$	$k_{v_2}$	$k_{v_3}$	$a_s$
1	15.3416	-	1.70872	-	16.8356
2	15.3225	-	1.87616	-	16.9627
3	15.2954	-	2.39856	-7.873	16.8264
4	15.5668	0.17993	1.28391	-	18.5295
$n$	$k_{s_1}$	$k_{s_2}$	$k_{s_3}$	$a_k$	$k_{k_1}$
1	-	1.40978	-	1.99142	-
2	-	2.94224	-	1.2545	-
3	-	7.85795	-73.9552	0.709782	-
4	1.46203	-2.1873	-	-2.72953	25.5927
$n$	$k_{k_2}$	$k_{k_3}$	$r_0$	$f_p$	$\sigma$
1	-	-	1.2205	1.33865	0.68
2	-50.7382	-	1.2281	1.28911	0.66
3	-395.7891	4557.60	1.2391	1.03047	0.61
4	-62.900	-	1.2285	0.91998	0.589

this adjustment to the nuclear masses the nuclear mass radius is not fitted. Root-mean-squared matter radii are given in ref. [25] for specific nuclei.

For the Bethe-Weizsäcker formula the fitting procedure leads to

$$B_{nucl}(A, Z) = 15.69A - 17.6037A^{2/3} - 0.71660 \frac{Z(Z-1)}{A^{1/3}} - 23.6745I^2 A + E_{pair} - E_{shell} \quad (8)$$

with  $\sigma=1.35$  MeV. That leads to  $r_0=1.2057$  fm and  $k_v=1.5089$ . The non dependence of the surface energy term on the relative neutron excess  $I$  explains the  $\sigma$  value.

The Fig. 1 shows the dispersion between the theoretical and experimental masses within the last formula presented in Table 2 and given below :

$$B = 15.5668 \left(1 - 0.17993|I| - 1.28391I^2\right) A - 18.5295 \left(1 - 1.46203|I| + 2.1873I^2\right) A^{\frac{2}{3}} + 2.72953 \left(1 - 25.5927|I| + 62.9I^2\right) A^{\frac{1}{3}} - \frac{3}{5} \frac{e^2 Z^2}{1.2285A^{\frac{1}{3}}} + 0.91998 \frac{Z^2}{A} + E_{pair} - E_{shell}. \quad (9)$$

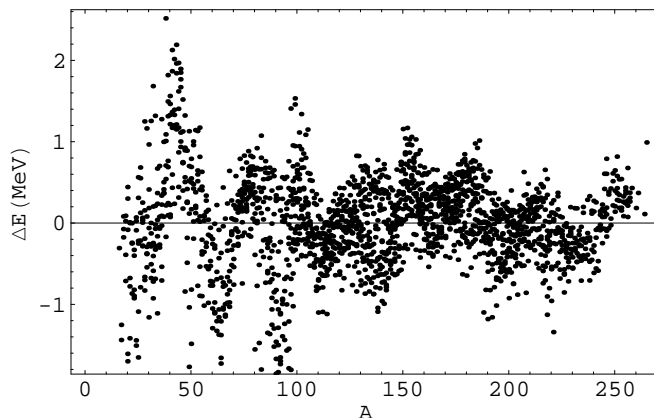


Figure 1: Difference (in MeV) between the theoretical and experimental masses for the 2027 nuclei as a function of the mass number.

### 3 SUMMARY AND CONCLUSION

The efficiency of different mass formulas derived from the liquid drop model and including or not a curvature energy term, the Wigner term and different powers of the relative neutron excess  $I$  has been determined by a least square fitting procedure to 2027 experimental atomic masses assuming a constant  $R_{0,charge}/A^{1/3}$  ratio. The Wigner term and the curvature energy term can improve independently the accuracy of the mass formula. The very satisfactory value of  $\sigma = 0.59$  MeV can be reached. The different fits lead to a volume energy coefficient of around 15.5 MeV, a surface energy coefficient of around 17-18 MeV, a relative charge radius  $r_0$  of 1.22-1.23 fm and a proton form-factor correction of around 0.9 MeV. The addition of a term in  $|I|$  in the volume, surface and curvature energy terms is more efficient than a term in  $I^4$ .

### References

- [1] C. F. von Weizsäcker, Z. Physik **96**, 431 (1935).
- [2] H. A. Bethe, R. F. Bacher, Rev. Mod. Phys. **8**, 82 (1936).
- [3] D. N. Basu, P. Roy Chowdhury, nucl-th/0408013.
- [4] P. Möller, J. R. Nix, W. D. Myers, and W. J. Swiatecki, At. Data Nucl. Data Tables **59**, 185 (1995).
- [5] W. D. Myers, W. J. Swiatecki, LBL Report 36803, 1994.

- [6] W. D. Myers, W. J. Swiatecki, Nucl. Phys. **A 601**, 141 (1996).
- [7] M. Samyn, S. Goriely, P.-H. Heenen, J. M. Pearson, and F. Tondeur, Nucl. Phys. **A 700**, 142 (2002).
- [8] J. Rikowska Stone, J. Phys. **G 31**, R211 (2005).
- [9] M. Bender et al, Phys. Lett. **B 515**, 42 (2001).
- [10] S. Athanassopoulos, E. Mavrommatis, K. A. Gernoth, and J. W. Clark, Nucl. Phys. **A 743**, 222 (2004).
- [11] R. W. Hasse, Ann. Phys., **NY 68**, 377 (1971).
- [12] G. Royer, B. Remaud, J. Phys. **G 10**, 1057 (1984).
- [13] G. Royer, B. Remaud, Nucl. Phys. **A 444**, 477 (1985).
- [14] G. Royer, J. Phys. **G 26**, 1149 (2000).
- [15] G. Royer, R. Moustabchir, Nucl. Phys. **A 683**, 182 (2001).
- [16] R. A. Gherghescu, G. Royer, Phys. Rev. **C 68**, 014315 (2003).
- [17] C. Bonilla, G. Royer, Heavy Ion Phys. **25**, 11 (2006).
- [18] G. Audi, A. H. Wapstra and C. Thibault, Nucl. Phys. **A 729**, 337 (2003).
- [19] D. Lunney, J. M. Pearson, and C. Thibault, Rev. Mod. Phys. **75**, 1021 (2003).
- [20] K. Pomorski, J. Dudek, Phys. Rev. **C 67**, 044316 (2003).
- [21] G. Royer, C. Gautier, Phys. Rev. **C 73**, 067302 (2006).
- [22] S. Hofmann et al, Z. Phys. **A 354**, 229 (1996).
- [23] W. D. Myers, *Droplet Model of Atomic Nuclei*, Plenum, New York, 1977.
- [24] I. Angeli, At. Data Nucl. Data Tables **87**, 185 (2004).
- [25] G. F. Lima et al, Nucl. Phys. **A 735**, 303 (2004).

## 4 APPENDIX



Table 3: Theoretical shell energy (in MeV) extracted from [5] (7<sup>th</sup> column) at the ground state of nuclei for which the half-life is higher than 1 ky.

<sup>16</sup> O	<sup>17</sup> O	<sup>18</sup> O	<sup>19</sup> F	<sup>20</sup> Ne	<sup>21</sup> Ne	<sup>22</sup> Ne	<sup>23</sup> Na
-0.45	1.19	1.3	2.76	2.81	2.82	2.19	2.22
<sup>24</sup> Mg	<sup>25</sup> Mg	<sup>26</sup> Mg	<sup>26</sup> Al	<sup>27</sup> Al	<sup>28</sup> Si	<sup>29</sup> Si	<sup>30</sup> Si
1.64	1.77	0.64	1.89	0.79	-0.26	-0.25	0.22
<sup>31</sup> P	<sup>32</sup> S	<sup>33</sup> S	<sup>34</sup> S	<sup>36</sup> S	<sup>35</sup> Cl	<sup>36</sup> Cl	<sup>37</sup> Cl
0.22	0.66	0.86	1.13	1.22	1.32	1.48	1.40
<sup>36</sup> Ar	<sup>38</sup> Ar	<sup>40</sup> Ar	<sup>39</sup> K	<sup>40</sup> K	<sup>41</sup> K	<sup>40</sup> Ca	<sup>41</sup> Ca
1.57	1.64	2.45	1.79	2.58	2.58	1.71	2.49
<sup>42</sup> Ca	<sup>43</sup> Ca	<sup>44</sup> Ca	<sup>46</sup> Ca	<sup>48</sup> Ca	<sup>45</sup> Sc	<sup>46</sup> Ti	<sup>47</sup> Ti
2.49	2.16	1.7	0.69	-0.82	2.43	2.44	1.95
<sup>48</sup> Ti	<sup>49</sup> Ti	<sup>50</sup> Ti	<sup>50</sup> V	<sup>51</sup> V	<sup>50</sup> Cr	<sup>52</sup> Cr	<sup>53</sup> Cr
1.44	0.81	-0.05	0.54	-0.31	0.74	-0.69	-0.38
<sup>54</sup> Cr	<sup>53</sup> Mn	<sup>55</sup> Mn	<sup>54</sup> Fe	<sup>56</sup> Fe	<sup>57</sup> Fe	<sup>58</sup> Fe	<sup>60</sup> Fe
0.74	-1.11	0.68	-1.54	0.05	0.72	1.22	2.07
<sup>59</sup> Co	<sup>58</sup> Ni	<sup>59</sup> Ni	<sup>60</sup> Ni	<sup>61</sup> Ni	<sup>62</sup> Ni	<sup>64</sup> Ni	<sup>63</sup> Cu
0.77	-1.58	-0.68	-0.16	0.59	1.1	1.63	1.86
<sup>65</sup> Cu	<sup>64</sup> Zn	<sup>66</sup> Zn	<sup>67</sup> Zn	<sup>68</sup> Zn	<sup>70</sup> Zn	<sup>69</sup> Ga	<sup>71</sup> Ga
2.33	2.53	2.89	3.16	2.99	2.94	3.79	3.71
<sup>70</sup> Ge	<sup>72</sup> Ge	<sup>73</sup> Ge	<sup>74</sup> Ge	<sup>76</sup> Ge	<sup>75</sup> As	<sup>74</sup> Se	<sup>76</sup> Se
4.13	4.08	4.19	3.82	2.53	4.08	4.42	4.08
<sup>77</sup> Se	<sup>78</sup> Se	<sup>79</sup> Se	<sup>80</sup> Se	<sup>82</sup> Se	<sup>79</sup> Br	<sup>81</sup> Br	<sup>80</sup> Kr
4.06	3.27	2.87	1.89	0.38	4.07	2.28	4.39
<sup>81</sup> Kr	<sup>82</sup> Kr	<sup>83</sup> Kr	<sup>84</sup> Kr	<sup>86</sup> Kr	<sup>85</sup> Rb	<sup>87</sup> Rb	<sup>86</sup> Sr
3.77	2.74	1.65	0.96	-0.40	1.13	-0.35	0.79
<sup>87</sup> Sr	<sup>88</sup> Sr	<sup>89</sup> Y	<sup>90</sup> Zr	<sup>91</sup> Zr	<sup>92</sup> Zr	<sup>93</sup> Zr	<sup>94</sup> Zr
0.05	-0.97	-1.19	-1.63	-0.47	0.46	1.53	2.54
<sup>96</sup> Zr	<sup>92</sup> Nb	<sup>93</sup> Nb	<sup>94</sup> Nb	<sup>92</sup> Mo	<sup>93</sup> Mo	<sup>94</sup> Mo	<sup>95</sup> Mo
3.49	-0.57	0.44	1.51	-2.12	-1.07	-0.12	0.97
<sup>96</sup> Mo	<sup>97</sup> Mo	<sup>98</sup> Mo	<sup>100</sup> Mo	<sup>97</sup> Tc	<sup>98</sup> Tc	<sup>99</sup> Tc	<sup>96</sup> Ru
1.79	2.46	2.98	3.62	1.26	2.05	2.64	-1.11
<sup>98</sup> Ru	<sup>99</sup> Ru	<sup>100</sup> Ru	<sup>101</sup> Ru	<sup>102</sup> Ru	<sup>104</sup> Ru	<sup>103</sup> Rh	<sup>102</sup> Pd
0.57	1.36	2.00	2.54	2.98	3.49	2.44	0.63
<sup>104</sup> Pd	<sup>105</sup> Pd	<sup>106</sup> Pd	<sup>107</sup> Pd	<sup>108</sup> Pd	<sup>110</sup> Pd	<sup>107</sup> Ag	<sup>109</sup> Ag
1.83	2.39	2.80	3.08	3.34	3.42	2.20	2.91
<sup>106</sup> Cd	<sup>108</sup> Cd	<sup>110</sup> Cd	<sup>111</sup> Cd	<sup>112</sup> Cd	<sup>113</sup> Cd	<sup>114</sup> Cd	<sup>116</sup> Cd
0.31	1.35	2.11	2.42	2.52	2.61	2.50	2.26
<sup>113</sup> In	<sup>115</sup> In	<sup>112</sup> Sn	<sup>114</sup> Sn	<sup>115</sup> Sn	<sup>116</sup> Sn	<sup>117</sup> Sn	<sup>118</sup> Sn
1.83	1.97	0.37	0.81	1.03	0.94	0.96	0.75
<sup>119</sup> Sn	<sup>120</sup> Sn	<sup>122</sup> Sn	<sup>124</sup> Sn	<sup>126</sup> Sn	<sup>121</sup> Sb	<sup>123</sup> Sb	<sup>120</sup> Te
0.70	0.19	-0.99	-2.51	-4.36	0.76	-0.16	2.08

<sup>122</sup> Te	<sup>123</sup> Te	<sup>124</sup> Te	<sup>125</sup> Te	<sup>126</sup> Te	<sup>128</sup> Te	<sup>130</sup> Te	<sup>127</sup> I
1.55	1.30	0.66	0.25	-0.62	-2.46	-4.74	0.35
<sup>129</sup> I	<sup>128</sup> Xe	<sup>129</sup> Xe	<sup>130</sup> Xe	<sup>131</sup> Xe	<sup>132</sup> Xe	<sup>134</sup> Xe	<sup>136</sup> Xe
-1.29	1.01	0.48	-0.31	-1.11	-2.36	-4.92	-7.2
<sup>133</sup> Cs	<sup>135</sup> Cs	<sup>132</sup> Ba	<sup>134</sup> Ba	<sup>135</sup> Ba	<sup>136</sup> Ba	<sup>137</sup> Ba	<sup>138</sup> Ba
-1.28	-3.90	0.93	-0.55	-1.45	-3.01	-4.18	-5.29
<sup>137</sup> La	<sup>138</sup> La	<sup>139</sup> La	<sup>136</sup> Ce	<sup>138</sup> Ce	<sup>140</sup> Ce	<sup>142</sup> Ce	<sup>141</sup> Pr
-2.22	-3.37	-4.50	0.70	-1.57	-3.86	-2.06	-3.26
<sup>142</sup> Nd	<sup>143</sup> Nd	<sup>144</sup> Nd	<sup>145</sup> Nd	<sup>146</sup> Nd	<sup>148</sup> Nd	<sup>150</sup> Nd	<sup>144</sup> Sm
-2.88	-2.14	-1.04	0.10	0.56	0.85	0.54	-2.28
<sup>146</sup> Sm	<sup>147</sup> Sm	<sup>148</sup> Sm	<sup>149</sup> Sm	<sup>150</sup> Sm	<sup>152</sup> Sm	<sup>154</sup> Sm	<sup>151</sup> Eu
-0.41	0.67	1.12	1.22	1.31	0.90	0.38	1.39
<sup>153</sup> Eu	<sup>150</sup> Gd	<sup>152</sup> Gd	<sup>154</sup> Gd	<sup>155</sup> Gd	<sup>156</sup> Gd	<sup>157</sup> Gd	<sup>158</sup> Gd
1.02	1.30	1.59	1.33	1.05	0.89	0.62	0.56
<sup>160</sup> Gd	<sup>159</sup> Tb	<sup>154</sup> Dy	<sup>156</sup> Dy	<sup>158</sup> Dy	<sup>160</sup> Dy	<sup>161</sup> Dy	<sup>162</sup> Dy
0.21	0.64	1.63	1.56	1.24	0.92	0.64	0.47
<sup>163</sup> Dy	<sup>164</sup> Dy	<sup>165</sup> Dy	<sup>163</sup> Ho	<sup>165</sup> Ho	<sup>162</sup> Er	<sup>164</sup> Er	<sup>166</sup> Er
0.16	-0.06	-0.41	0.46	-0.12	1.20	0.70	0.07
<sup>167</sup> Er	<sup>168</sup> Er	<sup>170</sup> Er	<sup>169</sup> Tm	<sup>168</sup> Yb	<sup>170</sup> Yb	<sup>171</sup> Yb	<sup>172</sup> Yb
-0.37	-0.54	-1.08	-0.60	0.32	-0.34	-0.76	-0.94
<sup>173</sup> Yb	<sup>174</sup> Yb	<sup>176</sup> Yb	<sup>175</sup> Lu	<sup>176</sup> Lu	<sup>174</sup> Hf	<sup>176</sup> Hf	<sup>177</sup> Hf
-1.32	-1.30	-1.74	-1.23	-1.62	-0.38	-0.90	-1.33
<sup>178</sup> Hf	<sup>179</sup> Hf	<sup>180</sup> Hf	<sup>182</sup> Hf	<sup>181</sup> Ta	<sup>180</sup> W	<sup>182</sup> W	<sup>183</sup> W
-1.53	-1.97	-1.99	-2.16	-2.02	-1.21	-1.71	-2.00
<sup>184</sup> W	<sup>186</sup> W	<sup>185</sup> Re	<sup>187</sup> Re	<sup>184</sup> Os	<sup>186</sup> Os	<sup>187</sup> Os	<sup>188</sup> Os
-2.02	-2.38	-2.19	-2.48	-1.61	-1.88	-2.16	-2.08
<sup>189</sup> Os	<sup>190</sup> Os	<sup>192</sup> Os	<sup>191</sup> Ir	<sup>193</sup> Ir	<sup>190</sup> Pt	<sup>192</sup> Pt	<sup>194</sup> Pt
-2.43	-2.47	-3.50	-2.54	-3.62	-0.97	-2.01	-3.31
<sup>195</sup> Pt	<sup>196</sup> Pt	<sup>198</sup> Pt	<sup>197</sup> Au	<sup>196</sup> Hg	<sup>198</sup> Hg	<sup>199</sup> Hg	<sup>200</sup> Hg
-4.04	-4.80	-6.11	-5.56	-4.51	-5.99	-6.75	-7.52
<sup>201</sup> Hg	<sup>202</sup> Hg	<sup>204</sup> Hg	<sup>203</sup> Tl	<sup>205</sup> Tl	<sup>202</sup> Pb	<sup>204</sup> Pb	<sup>205</sup> Pb
-8.37	-9.11	-10.69	-9.97	-11.58	-8.22	-10.02	-11.00
<sup>206</sup> Pb	<sup>207</sup> Pb	<sup>208</sup> Pb	<sup>208</sup> Bi	<sup>209</sup> Bi	<sup>226</sup> Ra	<sup>229</sup> Th	<sup>230</sup> Th
-11.82	-12.68	-12.84	-11.70	-11.95	-0.30	-0.52	-0.43
<sup>232</sup> Th	<sup>231</sup> Pa	<sup>233</sup> U	<sup>234</sup> U	<sup>235</sup> U	<sup>236</sup> U	<sup>238</sup> U	<sup>236</sup> Np
-0.60	-0.79	-1.27	-1.23	-1.46	-1.30	-1.27	-1.85
<sup>237</sup> Np	<sup>239</sup> Pu	<sup>240</sup> Pu	<sup>242</sup> Pu	<sup>244</sup> Pu	<sup>243</sup> Am	<sup>245</sup> Cm	<sup>246</sup> Cm
-1.74	-2.12	-1.95	-1.99	-2.08	-2.44	-3.05	-2.96
<sup>247</sup> Cm	<sup>248</sup> Cm	<sup>247</sup> Bk					
-3.17	-3.00	-3.46					